THE ASTROPHYSICAL JOURNAL, 350:186–194, 1990 February 10

HIGH ANGULAR RESOLUTION SUBMILLIMETER OBSERVATIONS OF SAGITTARIUS B2

PAUL F. GOLDSMITH AND DARIUSZ C. LIS
Five College Radio Astronomy Observatory, Department of Physics and Astronomy, University of Massachusetts at Amherst
AND
RICHARD HILLS AND JOAN LASENBY
MRAO, Cavendish Laboratory, Cambridge
Received 1989 April; accepted 1989 August 10

ABSTRACT

We have carried out continuum observations of the Sgr B2 molecular cloud at 1300 μm using the 14 m Five College Radio Astronomy Observatory (FCRAO) telescope, and at 1100, 850, 450, and 350 μm using the James Clerk Maxwell telescope (JCMT). These data, obtained with $\simeq 20''$ resolution, offer the first detailed description of the submillimeter radiation from this complex source. The emission is dominated by the middle and northern compact sources, but we have detected for the first time the far-infrared radiation associated with the Northeast H II region L of Benson and Johnston, as well as from the southern H II region/molecular maser source H. Our data, together with existing infrared measurements, indicate that the optical depth within Sgr B2(N) is significantly greater than that of Sgr B2(M) and that it has a noticeable effect for $\lambda \leq 800$ μm. The envelope of Sgr B2(M) becomes optically thick for the radiation from Sgr B2(N), located within it, for wavelengths ≤ 100 μm. From radiative transfer modeling, we obtain a luminosity of 10^7 $L_\odot$ for the middle source and 2×10^6 $L_\odot$ for the northern source.

Subject headings: galaxies: nuclei — interstellar: molecules — nebulae: individual (Sgr B2)

I. INTRODUCTION

Sagittarius B2 has long been recognized as an unusual molecular cloud in terms of the richness of the molecular spectrum and diversity of chemical species found in it. With respect to mass (6×10^6 $M_\odot$) and size (45 pc: Scoville, Solomon, and Penzias 1975; Lis and Goldsmith 1989), Sgr B2 is large, but it is well within the range of giant molecular clouds (GMCs) in the galaxy (see Solomon *et al.* 1987). However, these properties together indicate a mean molecular hydrogen density of 3000 cm^{-3}, a factor of 20–40 greater than is typical of disk clouds of the same size (Dame *et al.* 1986; Scoville *et al.* 1987), while the line-of-sight velocity dispersion is approximately 21 km s^{-1}, a factor of 7 greater than that of disk clouds of similar dimension (Solomon *et al.* 1987). The infrared properties of this region have also received considerable attention: its luminosity, 10^6–10^7 $L_\odot$, is high (see Goldsmith, Snell, and Lis 1987, hereafter GSL, and references therein), but the infrared emission to mass ratio is again well within the range found to characterize disk GMCs (Mooney and Solomon 1988).

The star formation process in Sgr B2 is an intriguing question. The rate at which newly formed stars are producing ionizing radiation is very large (see Benson and Johnston 1984); the interaction of these stars with their immediate surroundings is complex (Vogel, Genzel, and Palmer 1987) and the special environment of Sgr B2 near the Galactic Center may have an effect on the star formation taking place there. In addition, the unusually intense infrared emission and large dust column density characterizing Sgr B2 have been recognized for some time (Gezari, Joyce, and Simon 1973), but a detailed model capable of explaining the spectrum of the source remains problematic (Thronson and Harper 1986). To help clarify these issues, we have obtained a set of high angular resolution continuum maps of Sgr B2 at wavelengths between 350 and 1300 μm. The observing procedure and data are described in the following section. In § III, we present the cloud models developed to explain this and other infrared data available for this region, and in § IV we discuss the implications of the data and models.

II. OBSERVING PROCEDURE AND DATA

The 1300 μm data were taken in 1988 February and March using a dual polarization heterodyne system (Erickson 1986) on the 14 m FCRAO antenna; for further details of the data-taking procedure, see GSL. The choice of local oscillator frequency and double sideband operation results in spectral lines making a negligible contribution to the flux density in the 500 MHz wide IF passband. The typical system temperature referred to above Earth's atmosphere at the low elevations characteristic of Sgr B2 was 1400–2000 K. The antenna pointing and efficiency were verified by observations of Saturn at an elevation $\simeq 5°$ above that of Sgr B2. The FWHM was 23″, and the conversion from observed antenna temperature to unpolarized flux density 185 Jy K^{-1}, assuming a source temperature of 145 K (Werner *et al.* 1978).

The data consist of 45 positions with 15″ spacing and 16 positions with 20″ spacing centered at the position of the Sgr B2(M) continuum source ($\alpha_{1950} = 17^h44^m10^s.5$; $\delta_{1950} = -28°22'05''$). A contour map of the emission is shown in Figure 1*a*. The peak flux density of 56 Jy occurs at the (0, 50″) position, near the Sgr B2(N) continuum source, effectively the source denoted MD4 in the early interferometric study by Martin and Downes (1972). The flux density at Sgr B2(M) (which effectively is source MD5) is 44 Jy. All offsets are with respect to the position of Sgr B2(M). As discussed by GSL, the contribution of free-free emission can be estimated from lower frequency data to be approximately 25 Jy in a 60″ beam, less than 20% of the total flux density observed. The contribution of the free-free emission in small beams is approximately 5 Jy for both middle and north sources (Downes *et al.* 1976). The flux densities in different beam sizes observed at the Sgr B2(M)

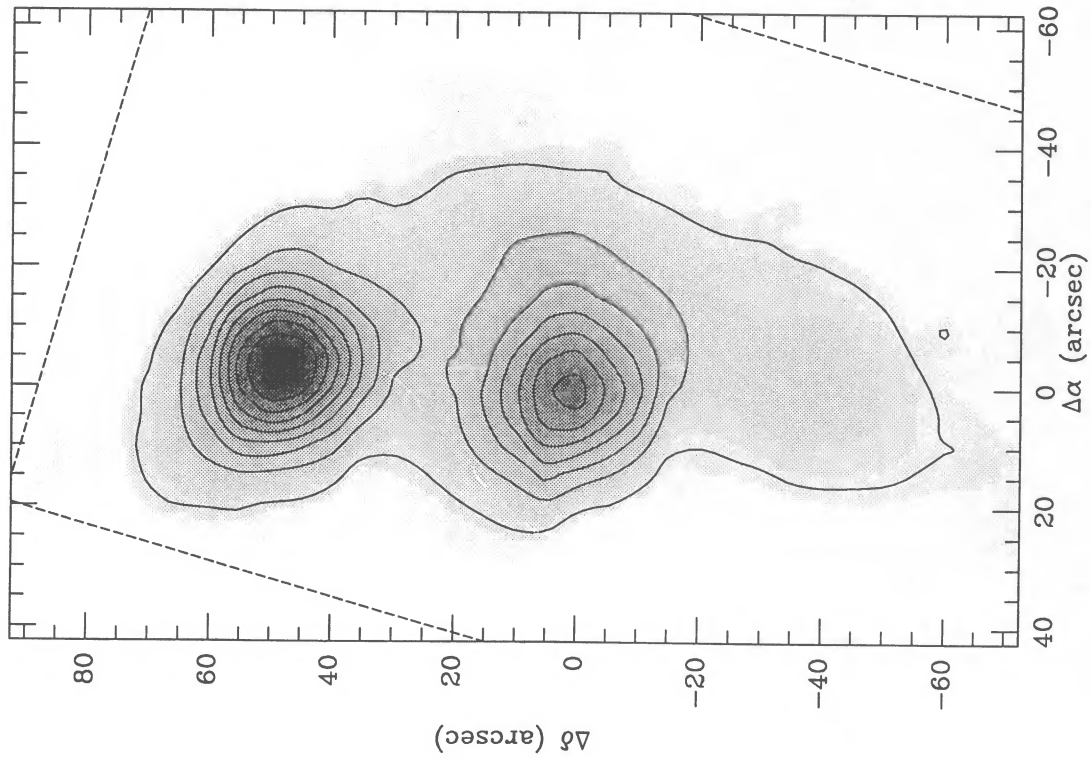

FIG. 1b

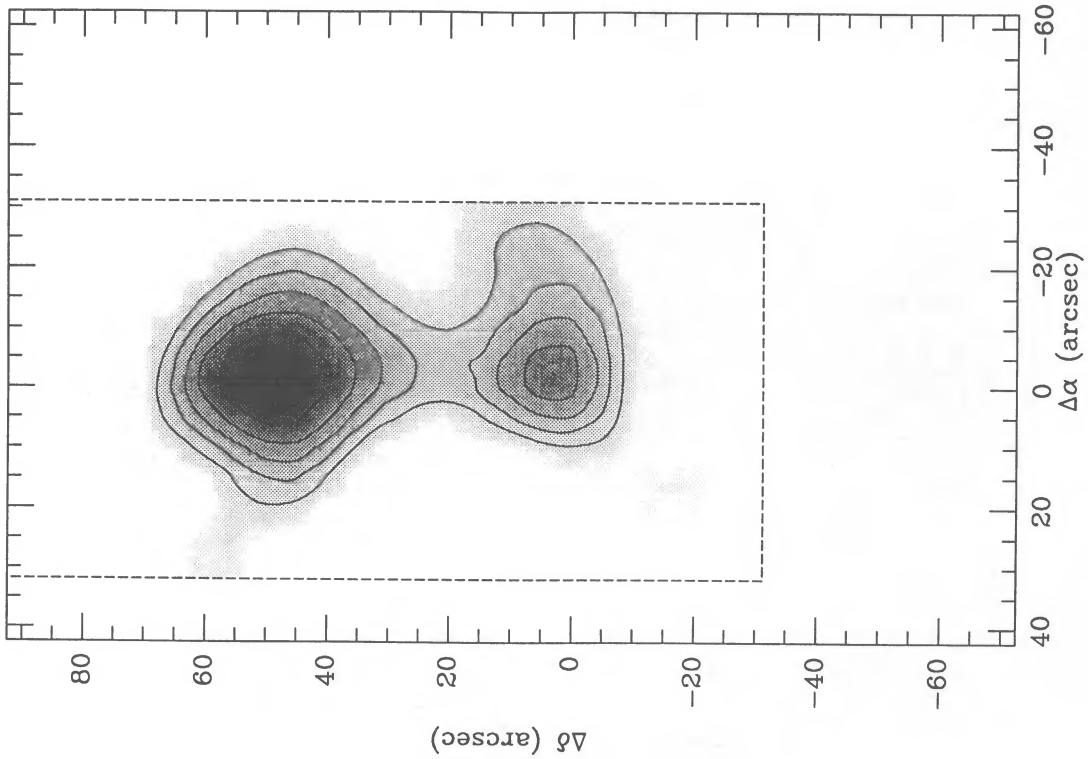

FIG. 1a

FIG. 1.—Maps of continuum radiation from the Sgr B2 molecular cloud. The (0, 0) position of all maps is the Sgr B2(M) continuum source ($\alpha_{1950} = 17^h44^m10^s5$; $\delta_{1950} = -28°22'05''$); the beam sizes and peak flux densities are given in Table 1. (*a*) 1300 μm distribution (FCRAO data) with contours at fractions 0.9, 0.8, 0.7, 0.6, and 0.5 of peak. (*b*)-(*e*) Distribution of flux density (JCMT data) at 1100, 800, 450, and 350 μm, respectively, with contours at fractions 0.9, 0.8, 0.7, 0.6, 0.5, 0.4, 0.3, 0.2, and 0.1 of peak in each map. These are 56, 103, 284, 1192, and 3962 Jy in the 1300 to 350 μm maps, respectively. Broken line in each map delineates the region for which data was obtained. The 350 μm map has had a bad row of data points replaced by interpolated values as discussed in the text.

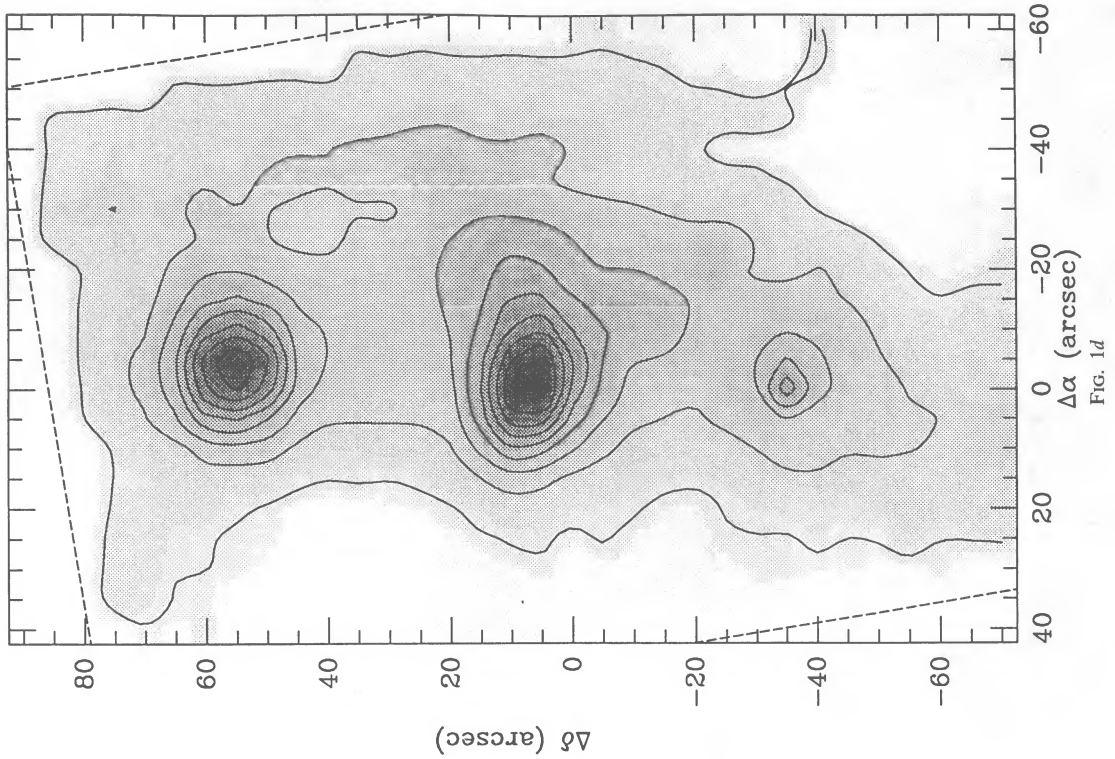

FIG. 1*d*

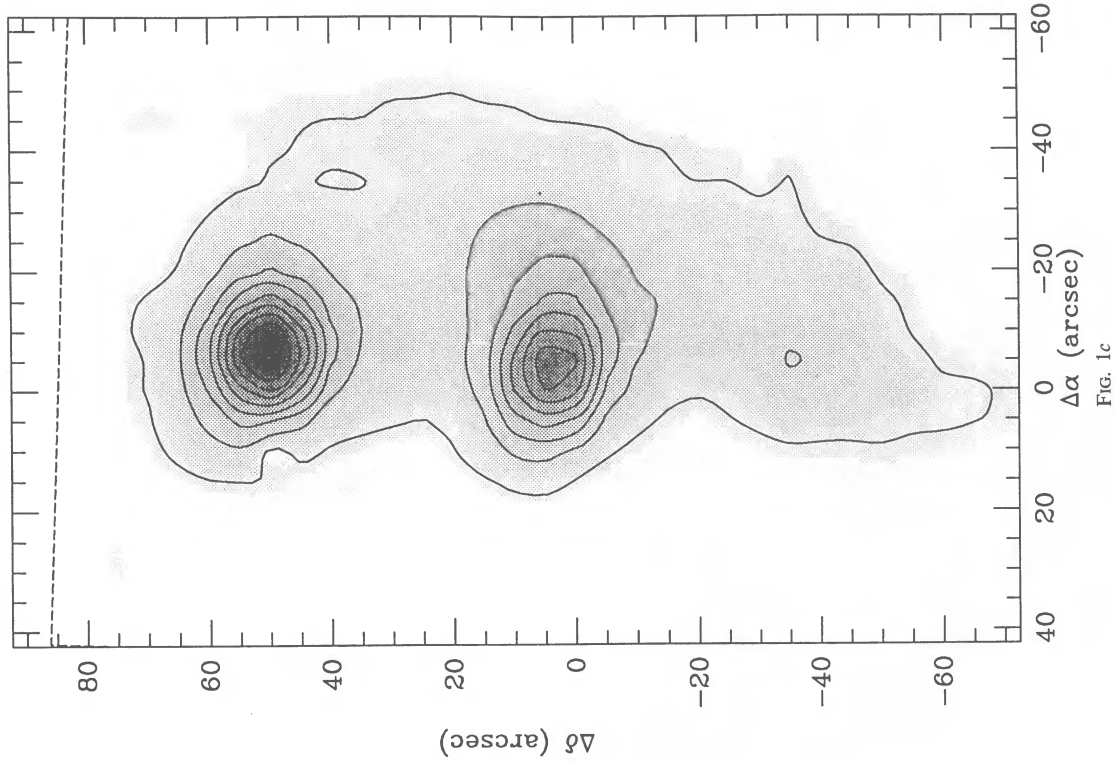

FIG. 1*c*

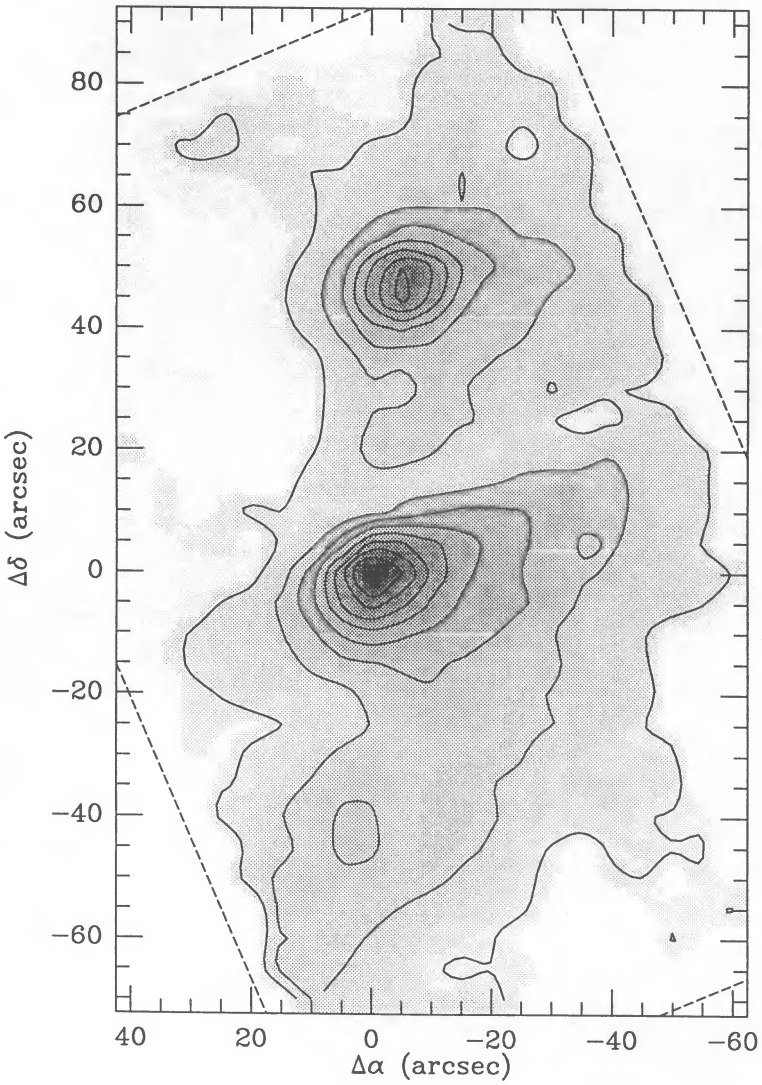

FIG. 1*e*

and (N) positions given in Table 1 include the contribution from free-free emission; the estimated values given above are subtracted before the models discussed below are fitted to the data. The peak flux densities measured here are consistent with those obtained previously by GSL and also by Gordon and Jewell (1987). The positional agreement between the 1300 μm peaks and the compact H II regions is good; the apparent offset in right ascension in Figure 8 of Gordon and Jewell is most likely the result of a transient pointing problem in their observations.

The data in the four shorter wavelength bands were obtained during the night of 1988 July 14/15, using the UKT14 bolometer system on the James Clerk Maxwell telescope. Cooled bandpass filters provided a resolving power of ≈ 5. The map in each band was obtained in the form of azimuth elevation raster scans, each having 33 × 33 points at 5″ spacing. The signal for each position was the difference obtained by chopping between the source and a reference position offset by 80″ in azimuth. Similar raster maps of Uranus (located less than 5° away from Sgr B2) for pointing and calibration were interspersed with observations of the source; the maximum pointing shift between two observations separated by $\simeq 30$ minutes in time was smaller than 4″. The flux density scale was established using the standard JCMT calibration program, which assumes brightness temperatures for Uranus of 92, 83, 71, and 66 K for the 1100, 800, 450, and 350 μm bands, respectively. These values are consistent with the measurement by Ulich, Dickel, and de Pater (1984) of $T_b = 101 \pm 11$ K at $\lambda = 1320$ μm, and $T_b = 71 \pm 9$ K at $\lambda = 410$ μm obtained by Lowenstein *et al.* (1977). Since the entire system response was calibrated by the Uranus measurements, we have no independent determination of the antenna efficiency.

The original data included the source in both the main and reference beams of the chopping secondary; the maps shown in Figure 1 were obtained by differencing the flux distribution in the two beams and then transforming each final map to a R.A.–decl. coordinate system. The beam size at each wavelength is given in Table 1, where we also present the flux densities integrated over different areas centered on Sgr B2(M) and Sgr B2(N). While contamination from spectral lines may be in principle a problem for broad-band observations, we do not feel it to be a significant issue in the present data. We estimate the

TABLE 1

OBSERVED FLUX DENSITIES IN DIFFERENT BEAM SIZES FROM Sgr B2(M) AND Sgr B2(N)[a]

Wavelength (μm)	Beam Size (″)	Observed Flux Density (Jy)	Flux Density in 30″ Beam (Jy)	Flux Density in 60″ Beam (Jy)[b]	Total Flux Density (Jy)[c]
		Sgr B2(M)			
1300.....	23	44	56	163	660[d]
1100.....	19[e]	79	105	210	530
800.....	16[e]	227	343	783	2248
450.....	16[e]	1192	1919	4686	14100
350.....	20[f]	3962	3780[g]	9090[g]	29600
		Sgr B2(N)			
1300.....	23	56	74	179	...
1100.....	19[e]	103	123	225	...
450.....	16[e]	1070	1646	4323	...
350.....	20[f]	3141	3173[g]	8370[g]	...

NOTE.—The total flux density includes the contributions from all sources.

[a] Uncertainties are dominated by calibration errors which are estimated to be $\pm 25\%$.

[b] The flux densities given here are not corrected for free-free emission; this effect is significant for the data in the two longer wavelength bands and is discussed in Section II in the text.

[c] These values are the total flux density in the region 1.′25 × 2.′25 for 1300 μm data and 1.′75 × 2.′75 for the shorter wavelength data. Consequently, as indicated in Fig. 1, the emission from both the middle and northern sources is included, but the extended emission present at the longer wavelengths is only partially incorporated.

[d] An additional uncertainty in integration of observed flux densities to obtain the total flux density is introduced by non-Gaussian components of the beam patterns. These close-in sidelobes and shoulders are a particularly significant problem for the longest and shortest wavelength observations, and they result in an overestimate of the total flux density. We feel that this effect is responsible for an excessive value of the total 1300 μm flux density. The millimeter-wavelength flux is probably most accurately determined from the 1100 μm data, for which the beam pattern is relatively clean, together with extrapolation to longer wavelengths if required.

[e] The 1100, 800, and 450 μm beams are highly Gaussian, but are elongated in the azimuth direction with major to minor axis ratio typically 1.2; the values given are the geometric mean FWHM beamwidths determined by fitting a two-dimensional Gaussian distribution.

[f] The beam shape at 350 μm wavelength is not very clean, containing a reasonably Gaussian central part, together with a highly elongated surrounding component. This makes the beam size determination necessarily imprecise.

[g] The original 350 μm data contained a row of bad pixels between the north and middle sources. These have been replaced by values interpolated from surrounding points. This factor, together with the uncertainty in the actual beam profile, is responsible for additional uncertainty in these values.

contribution (unchopped) flux density of the CO $J = 2$–1 transition to be only $\simeq 0.3$ Jy to the 1100 μm measurement of 81 Jy at Sgr B2(M), and the total contribution of 30 "strong" and 200 "weak" lines (based on compilation of Lovas 1987) to be only $\simeq 3$ Jy in this band. The contributions to our maps will be reduced further by the relatively small chopper throw compared to the angular extent of the emission from many species in Sgr B2. It does not appear likely that the integrated flux from spectral lines will rise as rapidly with frequency as the dust emission does, and thus we do not expect the shorter wavelength bands to be significantly affected.

Emission associated with a sourthern source located approximately 40″ South of Sgr B2(M) is seen in the 350 μm data, is prominent in the 450 μm map, and is detectable in the 800 μm and 1100 μm maps. Its flux density is approximately 8 Jy at 1100 μm, 60 Jy at 800 μm, 600 Jy at 450 μm, and 1400 Jy at 350 μm. A large part of the flux at the position of the southern source is emission from the extended component surrounding Sgr B2(M). Removal of this background does not significantly alter the spectral index of the emission, although the values of the flux densities are reduced by about a factor of 2. The southern source is the *only* discrete source detected at 20 μm in Sgr B2 by Downes (1988), having a flux density of 3.6 Jy, approximately a factor of 2 higher than the upper limits for Sgr B2(M) and Sgr B2(N). The relatively low flux at submillimeter wavelengths and greater strength in the infrared suggest a low-luminosity, low–column density source with moderate foreground extinction. The submillimeter peak agrees in position with Region H of Benson and Johnston (1984), for which they derive a luminosity of $4 \times 10^5\ L_\odot$, an order of magnitude lower than that of Sgr B2(M) and Sgr B2(N). The sparse infrared data prevent us from carrying out detailed modeling of this source at the present time.

The extension of the submillimeter continuum emission to the northeast of Sgr B2(N) in the 450 μm and 350 μm maps reaches approximately to the position of the compact H II region L observed by Benson and Johnston (1984) at 5 GHz, and at 15 GHz by Roelfsema *et al.* (1987). This source, located 40″ east and 70″ north of the (0, 0) position in Figure 1, has quite a large luminosity, $1.2 \times 10^6\ L_\odot$, implied by free-free emission (Benson and Johnston 1984).

III. SOURCE MODELS

The Sgr B2(M) and (N) sources are reasonably well resolved in our data. Taking advantage of the high-quality beams at 110 and 800 μm, we derive mean FWHM Gaussian diameters of

18″(0.75 pc) and 12″(0.5 pc) for the middle and northern sources, respectively. The latter is a factor of 2 larger than that obtained by Carlstrom and Vogel (1988) using 3.4 mm interferometer data. This may be a reflection of extended low-level emission resolved out by the interferometer and thus not reflected in their source size determination, as well as of limitations of the present measurements. Spatially extended emission, which peaks at the positions of the middle and northern sources, was found by Akabane *et al.* (1988) using high angular resolution single-dish observations at wavelengths of 1.3 and 0.7 cm.

An acceptable model for the northern and middle sources should reproduce the spectral distributions of the two components and their intensity ratio and should also be consistent with the molecular emission which probes the central region around the compact sources (especially $C^{18}O$; Lis and Goldsmith 1989*a*). A key parameter is the ratio of middle to northern source continuum flux density, which varies significantly with wavelength. The observed ratio is given in Table 2. The fact that the ratio increases as the wavelength decreases suggests that the increasing dust opacity is hiding the northern source from our view; the issue of which dust this is is discussed further in § IV. That the emission from Sgr B2(N) is *greater* at longer wavelengths probably indicates that in a small beam, the column density of dust is larger than in the middle source. Unlike Sgr B2(M), it does *not* show up as a peak in the $C^{18}O$ emission; this is because emission from this molecule is dominated by the inner, power-law portion of the envelope centered on Sgr B2(M), a fact which results in part from the high temperatures of the cores of both sources making the partition functions large, and the emission from the low-lying optically thin $J = 1$–0 transition relatively weak.

The coincidence of Sgr B2(M) with the $C^{18}O$ peak and its location at the center of the large-scale distribution of this molecule suggests that the overall dust distribution can be modeled as a spherically symmetric distribution. We have used the code of Egan, Leung, and Spagna (1988) to solve the radiative transfer problem. The dust emissivity is assumed to vary as λ^0 for wavelengths less than 0.1 μm, as λ^{-1} for $0.1 \geq \lambda \geq 100$ μm, and as $\lambda^{-1.5}$ for $\lambda > 100$ μm. A grain radius 0.1 μm, density $\rho = 3$ g cm^{-3}, and a gas-to-dust ratio of 100 by mass result in the parameter $Q/a\rho$ equal to 0.67 cm^2 g^{-1} at $\lambda = 1300$ μm. For a given density distribution of dust and central source luminosity, the temperature distribution and emission of the dust were calculated. In general, the results are similar to those obtained by Scoville and Kwan (1976), with the dust temperature being somewhat lower in the outer envelope owing to the high opacity. A distance to Sgr B2 of 8.5 kpc (a compromise between the IAU standard and the newer distance of 7.1 kpc determined by Reid *et al.* 1988) was adopted throughout this work. A change in the distance to the source directly affects the luminosity at a particular wavelength derived from observations. This translates in a complex manner to the parameters of the source model. One reason for this is that at different wavelengths, the radiated flux depends very differently on the luminosity of the heating source for the cloud. This issue is discussed in more detail by Lis and Goldsmith (1990).

TABLE 2

MIDDLE TO NORTH SOURCE FLUX DENSITY RATIOS

Wavelength (μm)	Observed in Actual Beam	Observed in 30″ Beam	Model in Actual Beam	Model in 30″ Beam
1300.....	0.80	...	0.80	0.86
1100.....	0.77	0.86	0.78	0.88
800.....	0.80	0.93	0.80	0.95
450.....	1.11	1.16	1.04	1.19
350.....	1.27	1.22	1.30	1.40
100.....	...	...	...	7.6
50.....	...	...	...	56.

NOTE:—The flux density ratios given here are not corrected for free-free emission, which makes a maximum contribution of about 20% to the flux at the longest wavelength measured in a large beam. Its importance in these small beam measurements is almost certainly less.

Recent observations of carbon monoxide isotopes with increased sensitivity (Lis and Goldsmith 1989) confirm earlier work by Scoville, Solomon, and Penzias (1975) which revealed Sgr B2 to have a large, centrally condensed envelope of moderate temperature. Based on molecular data (Lis and Goldsmith 1989), the extended cloud was modeled with two components: $n = n_1 + n_2$ for $r \leq r_0$, and $n = n_1[r/r_0]^{-2} + n_2$ for $R \geq r \geq r_0$, where n denotes the number density. In all models, the outer radius R of the cloud was taken equal to 22.5 pc (corresponding to 9′). The boundary of the central region of the cloud, r_0, was varied together with n_1 and n_2 in different models, with the best fits to the data being obtained for $r_0 \simeq 1.25$ pc (30″), $n_1 = 6.1 \times 10^4$ cm^{-3}, and $n_2 = 2.4 \times 10^3$ cm^{-3}.

The Sgr B2(M) core was represented by an additional Gaussian component: the small source size in the submillimeter continuum data suggests that the core size is significantly smaller than r_0. The core size, density, and central source luminosity were again varied in different models together with the envelope parameters to fit the observations at the different wavelengths in different beam sizes. Models with a FWHM core diameter d_c of 0.4 ± 0.1 pc were found satisfactory, together with peak core densities n_c within a factor of 2 of 4×10^6 cm^{-3}, and total source luminosities within a factor of 2 of 1.3×10^7 $L_\odot$.

The northern source has been modeled as a small clump of material situated within the Sgr B2(M) cloud; it was assumed to have dust with the same properties as given above and a Gaussian density distribution. Sgr B2(N) is located 45″ (1.85 pc) north of Sgr B2(M), and it was assumed to be located 5 pc behind the plane perpendicular to the line of sight containing Sgr B2(M); this places it behind most of the material in the envelope of Sgr B2(M); the exact location is not important for the present analysis, because the envelope is optically thin for $\lambda \leq 350$ μm. The radiation field within Sgr B2(N) was determined independently from that of Sgr B2(M), as a function of the luminosity, size, and central density of the northern source. The specific intensity along a given line of sight for the complete Sgr B2 model was calculated as the sum of two components: a contribution from the middle source and a contribution from the northern source attenuated by dust resulting from the extended component of the middle source. For a particular model of Sgr B2(M), the parameters of the northern source were varied to fit the middle-to-north flux density ratios at 1100 μm given in Table 2 (because the data quality at this wavelength is judged to be the highest). The observed and predicted flux densities in a 60″ beam at different wavelengths are shown in Figure 2, and the source parameters that we have adopted are given in Table 3.

IV. DISCUSSION

A significant result of the models of Sgr B2 is that the luminosity of the northern source is low, 1–2 $\times 10^6$ $L_\odot$, compared to $\simeq 10^7$ $L_\odot$ for the middle source. The northern source lumi-

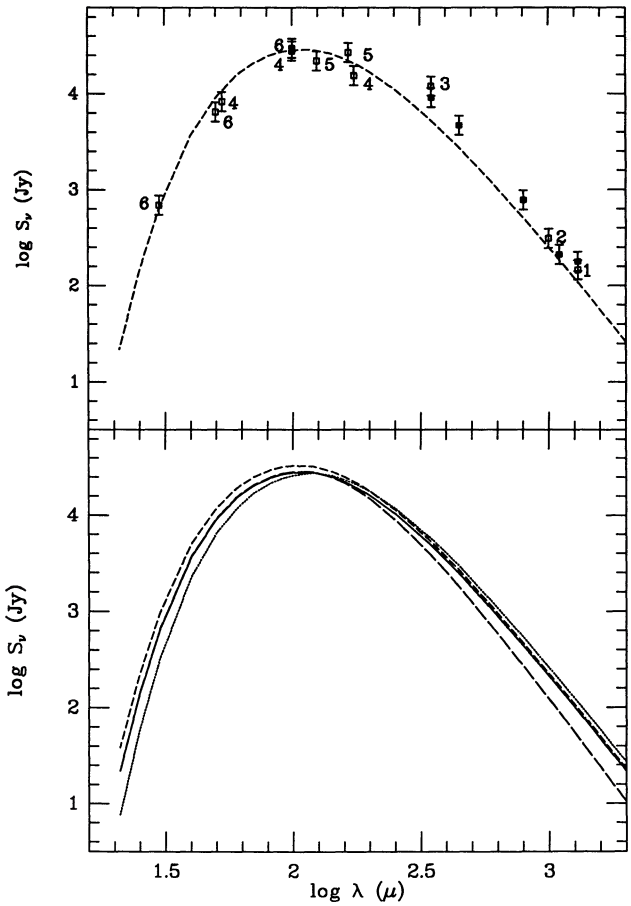

FIG. 2.—(*upper panel*) Flux density in 60″ beam centered on Sgr B2(M) predicted by model with parameters given in Table 3 (indicated by broken line), together with observations. For the latter, we have added a representative uncertainty of ±25%, indicative primarily of calibration errors. Data points are from the following sources: *filled squares*—present FCRAO and JCMT data; (1) previous FCRAO data from GSL; (2) Westbrook *et al.* (1976); (3) Righini, Simon, and Joyce (1976); (4) Harvey, Campbell, and Hoffmann (1977); (5) Thronson and Harper (1986); (6) Gatley *et al.* (1978). (*lower panel*) Effect of varying source and dust parameters on the flux density produced by a single, centrally heated source as discussed in § III of the text. Solid curve gives the spectral distribution produced by a source having luminosity $L = 7.5 \times 10^6\ L_\odot$, a dust optical depth from center to edge at 100 μm wavelength of 3.1, and a long-wavelength absorption efficiency factor varying as $\lambda^{-1.5}$. The parameters were varied individually with the short dashed curve indicating the effect of increasing the luminosity by 25%, the short dashed curve giving the effect of increasing the 100 μm optical depth by 25%, and the long dashed curve showing the variation produced by changing the power-law variation of the absorption to −1.75.

nosity is somewhat lower than that derived from centimeter free-free data by Benson and Johnston (1986), $\simeq 5 \times 10^6\ L_\odot$. The middle source luminosity is higher by a factor of 2 than derived by these authors from the radio free-free emission data.

TABLE 3

DERIVED PARAMETERS OF SGR B2 MIDDLE AND NORTH SOURCES[a]

	Sgr B2(M)	Sgr B2(N)
Envelope:		
n_1 (cm^{-3})	6.1×10^4	...
n_2 (cm^{-3})	2.4×10^3	...
r_0 (pc)	1.25	...
R (pc)	22.5	...
M ($M_\odot$)	6.9×10^6	...
Core:		
r_{in} (pc)	0.5	0.4
n_c (cm^{-3})	3.9×10^6	1.7×10^7
M ($M_\odot$)	2.9×10^4	6.4×10^4
L ($L_\odot$)	1.3×10^7	1.7×10^6

[a] The definitions of the envelope and core parameters are given in the text.

However, in view of the complexity of the different H II regions (see, e.g., discussion by Roelfsema *et al.* 1987 and Akabane *et al.* 1988), the issue of extended emission resolved out by interferometric observations, as well as possible calibration differences, the differences between the luminosities derived from radio free-free emission and our modeling of the submillimeter and infrared dust emission do not seem surprising.

The total luminosity of Sgr B2(M) together with Sgr B2(N) that we obtain is significantly lower than the $\simeq 7 \times 10^7\ L_\odot$ suggested by Thronson and Harper (1986). These authors suggest a model with an extensive, very cold foreground layer of dust which significantly attenuates the far-infrared emission from the source. Based on radiative transfer calculations, which are consistent with estimates from molecular column densities and a standard gas-to-dust-ratio, the envelope of Sgr B2(M) is optically thin for wavelengths less than 100 μm. Consequently, the variation in north to middle source flux ratio between $\lambda \simeq 1$ mm and $\lambda \simeq 400$ μm must be largely due to absorption by the dust *within the core of Sgr B2(N)*. Together with the greater long-wavelength flux, this leads to the conclusion, indicated by the numbers shown in Table 3, that the core of Sgr B2(N) has a considerably greater column density than

that of Sgr B2(M). The peak column density of 2.2×10^{25} cm^{-2} in Sgr B2(N) provides a center to edge optical depth of 8.8 at 100 μm and 1.3 at 350 μm, sufficient to attenuate the flux from the hot material very close to the center of the core.

The only readily apparent way to obtain significantly different relative luminosities for the middle and northern sources than found here is to have different wavelength dependences for the grain absorption efficiency in the two regions. The flux density in the infrared increases with increasing source luminosity but decreases with increasing optical depth (as seen in Fig. 2), so that we can lower the source luminosity by decreasing the opacity in this wavelength range. Since the flux density in the submillimeter scales essentially linearly with luminosity *and* submillimeter opacity, an increase in the ratio τ_{submm}/τ_{ir} together with a decrease in the source luminosity will leave the flux densities in both wavelength ranges unchanged.

Representative results for the effect on the emergent flux distribution produced by varying some of the key source parameters are given in Figure 2. As expected, the long-wavelength emission is strongly affected by the emissivity law, because this directly affects the opacity in this optically thin region. Changes in the source luminosity do not greatly affect the submillimeter/far-infrared continuum emission, which is an encouraging factor for use of these wavelengths to probe the mass distribution in extremely high column density clouds. Determination of the source luminosity requires observations at and shortward of the peak of the emission; with this information, the accuracy of the mass determined from the long-wavelength continuum emission can be enhanced.

We see from Table 2 that our source model explains the nondetection of Sgr B2(N) at 53 μm by Harvey, Campbell, and Hoffmann (1977); the observational lower limit on the middle to north source flux ratio is approximately 5. It is apparent that high-resolution 50 and 100 μm observations will help to determine the column density in front of Sgr B2(N) and thus its location and the density distribution within the Sgr B2(M) envelope.

The model given in Table 3 predicts a total flux of 41,600 Jy in a 4.5 beam at a wavelength of 160 μm, while Thronson and Harper (1986) measure 63,000 Jy in a map covering a comparable region. This agreement is quite good, given the observational uncertainties and especially the fact that we used a chopper with a throw of 1.33 and made no explicit attempt to recover the flux on larger spatial scales. The total flux density predicted by the model of Table 3 is 32 kJy at 350 μm and 22 kJy at 450 μm, only slightly higher than the observed values given in Table 1. Gezari, Joyce, and Simon (1973; with calibration modified by Righini, Simon, and Joyce 1976) measure 43,000–50,000 Jy in a 4.5 beam at 350 μm wavelength, compared to the model prediction of 13,000 Jy. The small chopping secondary throw that we used, the limited extent of the present data, and the severe problems of accurate calibration of ground-based 350 μm data prevent an entirely valid comparison of these values. For the same reasons, the present data are not particularly well-suited for comparison with total flux densities predicted by the model at even longer wavelengths. The total flux density predicted by the model is 6.1 kJy at 800 μm, 2.6 kJy at 1100 μm, and 1.6 kJy at 1300 μm, considerably in excess of the integrated flux densities presented in Table 1. If future data confirm that the flux density predicted by the model is inadequate, the most likely modification required would be to raise the temperature in the outer parts of the envelope, which could be done without significantly affecting any of the data presently fitted. This could be the result of grain properties being different from those used in the radiative transfer calculations, or of enhanced grain heating in the environment close to the galactic center.

V. CONCLUSIONS

We have carried out high angular resolution continuum observations at wavelengths between 1300 and 350 μm of Sagittarius Sgr B2. We have been able to resolve the two most prominent peaks, the middle and northern H II region complexes, and have detected for the first time emission in this wavelength range associated with southern and northeastern H II regions. We have carried out radiative transfer calculations for a model in which Sgr B2(N) is embedded in the envelope of a centrally condensed cloud having Sgr B2(M) at its center. The middle to north source flux ratio is less than unity in the $\simeq 1$ mm wavelength range. This ratio increases at shorter wavelengths, where the envelope of the middle source should still be optically thin. The best explanation is that the northern source has a larger column density than the mddle source, and is becoming optically thick to its own radiation for $\lambda \leq 800$ μm. At wavelengths ≤ 100 μm the envelope of Sgr B2(M) also becomes optically thick, resulting in an extremely large middle to north source flux ratio. We determine the luminosity of the middle source to be 1.3×10^7 $L_\odot$, and that for the northern source to be 1.7×10^6 $L_\odot$. Adopting standard grain parameters, we find the maximum H_2 column density in the envelope of Sgr B2(M) to be 1.3×10^{24} cm^{-2}, and the total mass of the 22.5 pc diameter cloud to be 7×10^6 $M_\odot$.

The Five College Radio Astronomy Observatory is supported by the Commonwealth of Massachusetts and the National Science Foundation under Grant AST 85-12903 and is operated with the permission of the Metropolitan District Commission. The JCMT is operated by the Royal Observatory, Edinburgh, on behalf of the Science and Engineering Research Council of the United Kingdom, the Netherlands Organization for Scientific Research, and the National Research Council of Canada. We acknowledge travel support from the National Radio Astronomy Observatory for P.F.G., and allocation of time and support by the PATT and SERC. We thank D. Downes for providing unpublished data and for a valuable discussion concerning Sgr B2, and C. Leung for providing us with a copy of his radiative transfer program. This is contribution 688 of the FCRAO and the Five College Astronomy Department.

REFERENCES

Akabane, K., Sofue, Y., Hirabayashi, H., Morimoto, M., and Inoue, M. 1988, *Pub. Astr. Soc. Japan*, **40**, 459.
Benson, J. M., and Johnston, K. J. 1984, *Ap. J.*, **277**, 181.
Carlstrom, J. E., and Vogel, S. N. 1988, *Ap. J.*, **337**, 408.
Dame, T. M., Elmegreen, B. G., Cohen, R. S., and Thaddeus, P. 1986, *Ap. J.*, **305**, 892.
Downes, D. 1988, private communication.
Downes, D., Goss, W. M., Schwarz, U. J., and Wouterloot, J. G. A. 1976, *Astr. Ap. Suppl.*, **35**, 1.
Egan, M. P., Leung, C. M., and Spagna, G. F. 1988, *Computer Phys. Comm.*, **48**, 271.
Erickson, N. R. 1986, *IEEE Trans. MTT*, **MTT-33**, 1179.
Gatley, I., Becklin, E. E., Werner, M. W., and Harper, D. A. 1978, *Ap. J.*, **220**, 22.

Gezari, D. Y., Joyce, R. R., and Simon, M. 1973, *Ap. J. (Letters)*, **179**, L67.
Goldsmith, P. F., Snell, R. L., and Lis, D. C. 1987, *Ap. J. (Letters)*, **313**, L5 (GSL).
Gordon, M. A., and Jewell, P. R. 1987, *Ap. J.*, **323**, 766.
Harvey, P. M., Campbell, M. F., and Hoffmann, W. F. 1977, *Ap. J.*, **211**, 786.
Lis, D. C., and Goldsmith, P. F. 1989, *Ap. J.*, **337**, 704.
———. 1990, in preparation.
Lovas, F. J. 1987, *J. Phys. Chem. Ref. Data*, **15**, 251.
Lowenstein, R. F., *et al.* 1977, *Icarus*, **31**, 315.
Martin, A. H. M., and Downes, D. 1972, *Ap. Letters*, **163**, 299.
Mooney, T. J., and Solomon, P. M. 1988, *Ap. J. (Letters)*, **334**, L51.
Reid, M. J., Schneps, M. H., Moran, J. M., Gwinn, C. R., Genzel, R., Downes, D., and Ronnang, B. 1988, *Ap. J.*, **330**, 809.
Righini, G., Simon, M., and Joyce, R. R. 1976, *Ap. J.*, **207**, 119.
Roelfsema, P. R., Goss, W. M., Whiteoak, J. B., Gardner, F. F., and Pankonin, V. 1987, *Astr. Ap.*, **175**, 219.
Scoville, N. Z., and Kwan, J. 1976, *Ap. J.*, **206**, 718.
Scoville, N. Z., Solomon, P. M., and Penzias, A. A. 1975, *Ap. J.*, **201**, 352.
Scoville, N. Z., Yun, M. S., Clemens, D. P., Sanders, D. B., and Waller, W. H. 1987, *Ap. J. Suppl.*, **63**, 811.
Solomon, P. M., Rivolo, A. R., Barrett, J., and Yahil, A. 1987, *Ap. J.*, **319**, 730.
Thronson, H. A., and Harper, D. A. 1986, *Ap. J.*, **300**, 396.
Ulich, B. L., Dickel, J. R., and de Pater, I. 1984, *Icarus*, **60**, 590.
Vogel, S. N., Genzel, R., and Palmer, P. 1987, *Ap. J.*, **316**, 243.
Werner, M. W., Neugebauer, G., Houck, J. R., and Hauser, M. G. 1978, *Icarus*, **35**, 289.
Westbrook, W. E., *et al.* 1976, *Ap. J.*, **209**, 94.

PAUL F. GOLDSMITH and DARIUSZ C. LIS: Five College Radio Astronomy Observatory, Department of Physics and Astronomy, 619 Graduate Research Tower, University of Massachusetts, Amherst, MA 01003

RICHARD HILLS and JOAN LASENBY: Mullard Radio Astronomy Observatory, Cavendish Laboratory, Madingley Road, Cambridge CB3 0HE, Great Britain